

# An X-ray and Optical Study of Matter Distribution in the Galaxy Cluster A 2319

D.Trèvese, G. Cirimele, and M. De Simone

Istituto Astronomico, Università di Roma “La Sapienza”, via G.M. Lancisi 29, I-00161 Roma,  
Italy;  
trevese@astro.uniroma1.it

Accepted for publication on *Astrophys. J.*

## ABSTRACT

A new analysis of velocity distribution, optical photometry and X-ray surface brightness from ROSAT PSPC data of the galaxy cluster A 2319 is presented. The temperature profile derived from ASCA data (Markevitch 1996) is taken into account. A method to check the hydrostatic model in the presence of a temperature gradient is proposed. Consistency of the hydrostatic isothermal model and the explanation of the “ $\beta$ -discrepancy” are discussed. Galaxy and gas density profiles of the main component A 2319 A are derived, allowing for the effect of the secondary component A 2319 B. The inadequacy of a polytropic model, which would produce a binding mass decrease with respect to the isothermal  $\beta$ -model, is discussed. A simple interpolation of the temperature profile provides instead an increase of the binding mass and a lower baryon fraction thus mitigating the “baryon catastrophe”. Assuming as typical the value  $f_b \approx 0.2$ , a comparison with the most recent estimate of  $\Omega_b^{nucl}$  implies for the cosmological parameter  $\Omega_o \lesssim 0.4$ .

*Subject headings:* dark matter – galaxies: clusters: individual (A 2319) – galaxies: photometry – intergalactic medium – X-ray: galaxies

## 1. Introduction

Detailed studies of the matter distribution in clusters of galaxies provide important clues on the growth of condensations and the evolution of the Universe. From X-ray observations it is possible to derive both the gas and the total binding mass distributions, under the assumption of hydrostatic equilibrium. Optical data, i.e. galaxy photometry and redshifts, combined with X-ray observations allow to check the validity of the hydrostatic equilibrium assumption and derive the spatial distribution of the dark matter. Most analyses in the past (Jones and Forman 1984, Cowie, Henriksen and Mushotzky 1987, Hughes, Gorenstein and Fabricant 1988, Hughes 1989, Gerbal

et al. 1992, Briel, Henry and Böhringer 1992, Durret et al. 1994, David, Jones and Forman 1995, Cirimele, Nesci and Trèvese 1997) were based on the further simplifying assumption that the gas is isothermal, at least within about  $1 h_{50}^{-1}$  Mpc, possibly with the exclusion of a central cooling flow region (see e.g. Fabian, Nulsen and Canizares 1984, White, Jones and Forman 1997). This leads to the  $\beta$ -model (Cavaliere and Fusco-Femiano 1976) which predicts that the dynamical parameter  $\beta_{spec} \equiv \frac{\mu m_p \sigma_r^2}{kT}$ , representing the ratio between the energy per unit mass of galaxies and gas, equals the morphological parameter  $\beta_{fit}$  defined by the fit of the gas density distribution with a King profile. The observations show that on average  $\beta_{fit} < \beta_{spec}$  (Sarazin 1986, Evrard 1990). However Bahcall and Lubin (1994) ascribed this "β-discrepancy" to the underestimate of the slope of the galaxy density profile, appearing in the hydrostatic equilibrium equation, rather than to a failure of the model. In their X-ray–Optical analysis of a sample of Abell clusters, Cirimele, Nesci, & Trèvese (1997) (CNT) found that  $\log \rho_{gas} = \beta_{XO} \log \rho_{gal} + C$  in a wide range of densities, as predicted by the hydrostatic isothermal equilibrium. This allows to define, for each cluster, a morphological parameter  $\beta_{XO}$ , independent of any analytical representation of  $\rho_{gas}$  and  $\rho_{gal}$ . A comparison of  $\beta_{XO}$  with  $\beta_{spec}$  supports the explanation of the "β-discrepancy" suggested by Bahcall and Lubin 1994 and the consistency of the "β-model", at least for several galaxy clusters of regular and relaxed appearance. The gas and binding mass distributions thus derived provide a typical value of the baryon fraction  $f_B$ , of the order of 0.2 within  $1-2 h_{50}^{-1}$  Mpc (Cirimele, Nesci and Trèvese 1997, Evrard 1997, Ettori & Fabian 1999, Mohr et al., 1999). This relatively high value, compared with the results of primordial nucleosynthesis calculation (Walker et al. 1991, Olive, Steigman 1995, but see Burles and Tytler 1998) implies that either the cosmological parameter is smaller than unity (White et al. 1993), or  $f_B$  is not representative of the cosmic value, and galaxy clusters are surrounded by extended halos of non baryonic dark matter (White and Fabian 1995). The latter hypothesis raises the problem of understanding the mechanisms of a large scale baryonic segregation.

However, recently ASCA data have provided direct evidences of gas temperature gradients in the outer regions of several galaxy clusters (Arnaud 1994, Markevitch et al. 1994, Markevitch et al. 1996, Ikebe et al. 1996, Markevitch 1996, Markevitch et al. 1998). According to Markevitch 1996, in the outer regions some clusters show a polytropic index even greater than  $5/3$ , which is inconsistent with the hydrostatic equilibrium conditions. According to Ettori & Fabian (1998), a systematic difference between the electron and the proton temperatures cannot explain the inconsistency, and a real departure from hydrostatic equilibrium must happen in some cases. Even disregarding these extreme cases, once the temperature profiles are available it is worth: i) to check how far from the cluster center the hydrostatic condition can be assumed, specially if strong temperature gradients are present; ii) to estimate the correction to the total mass and baryon fraction implied by non-isothermality. Moreover some clusters show an anomalously high value of the dynamical parameter  $\beta_{spec}$ , possibly suggesting deviations from the equilibrium conditions and requiring a detailed analysis of the velocity distribution. The galaxy cluster A 2319 has been extensively studied in the past, so that many galaxy redshifts are available, ROSAT PSPC images can be retrieved from the public archive and a temperature profile based on ASCA data has been

published by Markevitch 1996 (see however Molendi 1998, Molendi et al. 1999).

In the present work we combine these data with the F band photometry of galaxies (Trèvese et al. 1992), and compare the gas and galaxy density distributions. We generalize the definition of the morphological parameter  $\beta_{XO}$  to verify the hydrostatic equilibrium conditions. The analysis suggests the consistency of the hydrostatic model in the presence of a temperature gradient. Thus we discuss the mass distribution as obtained by adopting a polytropic model or a simple parabolic representation of the temperature profile, and we compare the resulting baryon fraction with the limits provided by the standard nucleosynthesis calculations, then deriving constraints on the large scale baryon segregation and the cosmological parameter  $\Omega_o$ .

We use  $H_o = 50 h_{50} \text{ km s}^{-1} \text{ Mpc}^{-1}$ .

## 2. The galaxy distribution

The galaxy cluster A 2319 has been studied by several authors in the radio, optical and X-ray bands. It is classified as a BM type II-III and as a richness 1, RS-type cD cluster (see Abell, Corwin and Olowin 1989). The galaxy velocity dispersion  $\sigma \approx 1800 \text{ km s}^{-1}$  is particularly high. However, Faber and Dressler (1977), on the basis of 31 galaxy spectra already suggested that A 2319 is actually two clusters nearly superimposed along the line of sight: the main component A 2319 A with an average redshift  $\bar{v}_A = 15882$  and a velocity dispersion  $\sigma_A = 873_{-148}^{+131} \text{ km s}^{-1}$  and the second component A 2319 B, located about 8' NW with  $\bar{v}_B = 19074$  and  $\sigma_B = 573_{-149}^{+120} \text{ km s}^{-1}$ .

More recently Oegerle, Hill, and Fitchett (1995)(OHF) measured several new redshifts, applied the "δ-test" of Dressler and Shectman (1988) to locate the A and B components, and assigned the 139 galaxies of known redshift to the component A and B (or to the background/foreground) on the basis of their position and redshift, empirically trying to keep gaussian the velocity distribution of A 2319 B. They found  $N_A = 100$  and  $N_B = 28$  galaxies in the two components with  $\bar{v}_A = 15727 \text{ km s}^{-1}$ ,  $\sigma_A = 1324 \text{ km s}^{-1}$   $\bar{v}_B = 18636 \text{ km s}^{-1}$   $\sigma_B = 742 \text{ km s}^{-1}$  respectively.

To assign individual galaxies to the A and B components we adopted the results of OHF to obtain a first order estimate of the cluster positions, average radial velocities  $\bar{v}^{(i)}$ , and velocity dispersions  $\sigma_{(i)}$ , and we computed the relevant core radii  $R_c^{(i)}$  of the two components, where  $i = A, B$  identifies the component. Then we assumed the following probability distributions of galaxies respect to radial velocities  $v$  and projected distance  $b$  from the relevant cluster center:

$$\begin{aligned}
 P_i(b, v) &\equiv \frac{N_i}{N_A + N_B} \cdot f_i(b) \cdot g_i(v) \\
 f_i(b) &= \left\{ \frac{2\pi R_c^{(i)2}}{1 - \beta_{(i)}} \left( \left[ 1 + \left( \frac{b_{max}^{(i)}}{R_c^{(i)}} \right)^2 \right]^{(1-\beta_{(i)})} - 1 \right) \right\}^{-1} \left[ 1 + \left( \frac{b}{R_c^{(i)}} \right)^2 \right]^{-\beta_{(i)}}
 \end{aligned} \tag{1}$$

$$g_i(v) = \frac{1}{\sqrt{2\pi\sigma_{(i)}^2}} \exp\left[-\frac{(v - \bar{v}_{(i)})^2}{2\sigma_{(i)}^2}\right]$$

where  $N_{(i)}$  the first order estimate of the number of galaxies of the relevant component, and the  $b_{max}^{(i)}$  is the radius of the circle containing the  $N_i$  observed galaxies. This simple parameterization is independent of any assumption about the distance along the line of sight of the two clusters and their relative motion. Each galaxy is then assigned to the component of higher probability. The 99% confidence volumes are also considered for each cluster, and galaxies outside these volumes are assigned to the background or foreground. We obtain the new values  $N_A=96$  and  $N_B=24$   $\bar{v}_A = 15891 \text{ km s}^{-1}$ ,  $\sigma_A = 1235 \pm 90 \text{ km s}^{-1}$ ,  $\bar{v}_B = 18859 \text{ km s}^{-1}$ ,  $\sigma_B = 655 \pm 97 \text{ km s}^{-1}$ . Since the resulting velocity distributions of the two components do not show strong deviation from gaussian distributions, the reported uncertainties  $\sigma_{\sigma_A}$  and  $\sigma_{\sigma_B}$ , on  $\sigma_A$  and  $\sigma_B$  respectively, have been computed as  $\sigma_{\sigma_i}^2 = \sigma_{(i)}^2/[2(N_{(i)} - 1)]$   $i=A,B$ . The effect of membership uncertainty can be evaluated as follows. Given a sample of  $N$  galaxies with average velocity  $\bar{v}$  and velocity dispersion  $\sigma$ , the addition of  $k$  galaxies with velocity  $v = \bar{v} + \delta$  produces a new velocity dispersion  $\sigma'^2 = (N\sigma^2 + k\delta^2)/(N + k - 1)$ . Therefore, to increase  $\sigma_A$  by more than  $2\sigma_{\sigma_A}$  it is necessary to include in the sample A more than  $k=2$  galaxies with a recession velocity exceeding  $\bar{v}_B + 2\sigma_B \simeq \bar{v}_A + 3.46\sigma_A$ .

Although on the sole basis of the " $\delta$  test" there is a 10% probability that A2319B is not a physical association, the strong clustering of large  $\delta$  values in a region (see OHF fig.5) corresponding to enhanced X-ray emission suggest that it is a physical entity. Moreover, the analysis of bound orbits of the two components A 2319 A and A 2319 B led Oegerle, Hill, and Fitchett 1995 to the conclusion that "there is a reasonably high probability that these clusters are not bound and will never merge". The latter conclusion is supported by the discussion of FGB who compare the X-ray images with simulations of cluster collisions (see section 3). The above considerations suggest and legitimate the assumption, adopted in the following, that the two clusters are separate entities.

We have added to the spectroscopic information the F band photometry of A 2319, obtained by Trèvese et al. 1992 from microdensitometric scans of a Palomar 48 inch Schmidt plates, as part of a systematic study of the morphology and luminosity functions of galaxy clusters (Trèvese, Cirimele and Flin 1992, Flin et al. 1995, Trèvese, Cirimele and Appodia 1996, Trèvese et al. 1997). Due to the low galactic latitude ( $b \simeq 13^\circ$ ) the field of A 2319 is very crowded and the automatic star/galaxy classification is difficult. Thus we have revised the classification and recovered some misclassified object.

To focus our attention on the main component A, we reduced the effect of the B component excluding from our sample all the galaxies classified as B (or background/foreground). We adopted a fixed center ( $\alpha = 19^h 21^m 11.8^s$ ,  $\delta = +43^\circ 56' 39''$  (J2000)), derived from the centroid of X-ray emission as computed in a small (2 arcmin) circle around the intensity peak. This point is identified with the center of a spherical structure which we assume to represent the A component.

We chose a magnitude limit  $m_F = m_3 + 2 = 16.33$  mag and the resulting fraction of galaxies without measured redshift is 0.23. Thus, the fraction of galaxies without measured redshift and belonging to the B component is of the order  $0.23N_B/(N_A + N_B)$ , i.e. 4%, and is not expected to affect significantly the galaxy density profile. We fitted with a maximum likelihood algorithm the unbinned galaxy distribution using both a King profile  $\sigma_{gal}(b) = \sigma_0 \cdot (1 + (b/r_c)^2)^{-\kappa} + \sigma_b$  and with a de Vaucouleurs profile  $\sigma_{gal}(b) = \sigma_0 \cdot \exp(-7.67(b/r_v)^{\gamma_g}) + \sigma_b$ , where the background counts  $\sigma_b$ ,  $r_v$ ,  $\gamma_g$ ,  $r_c$  and  $\beta$  are free parameters, while  $\sigma_0$  is determined by the normalization to the total number of observed galaxies and  $b$  is the projected distance from the cluster center. The Kolmogorov-Smirnov (KS) test has been applied in both cases and the results are reported in Table 1, where the errors reported represent one-sigma uncertainties derived from Monte Carlo simulations described in section 4, and  $P_{KS}(> D)$  is the probability of the null hypothesis that deviations larger than  $D$  are produced by random noise.

The surface density and the fitting profiles are shown in Figure 1. In this case the King profile has a slightly higher probability and will be adopted in the following to derive the volume distribution by numerical inversion. However, the differences between the two fitting curves, specially for  $b > 0.1h_{50}^{-1} Mpc$ , cannot affect significantly the subsequent discussion of the hydrostatic equilibrium conditions.

To obtain the total luminosity of the cluster,  $L_{tot}(r)$ , we fitted with a Schechter (1976) function the unbinned luminosity distribution excluding the brightest member, using a maximum likelihood algorithm, adopting a constant  $\alpha = -1.25$  and  $M^*$  as a free parameter, as in Trèvese, Cirimele and Appodia 1996. This gives:

$$L_{tot}(r) = 10^{-0.4(M_F^* + 28.43)} \frac{\Gamma(2 + \alpha) \cdot 4\pi}{\Gamma(1 + \alpha, \frac{L_{lim}}{L^*})} \cdot \int_0^r \rho_{gal}(r') r'^2 dr' \quad (2)$$

where  $L_{tot}$  is expressed in units of  $10^{13}L_\odot$ ,  $r$  in  $kpc$  and  $L_{lim}$  is the limiting luminosity corresponding to the magnitude limit ( $M_F = -21.56$  mag) of the galaxy sample adopted to derive  $\rho_{gal}$ . The value of  $M^*$  changes by less than 1% considering a sample which includes the galaxies of A 2319 B. The galaxy mass  $M_{gal}(r)$  is then obtained from the total luminosity assuming an average mass-to-light ratio  $M/L_R = 3.32 \pm 0.14M_\odot/L_{R\odot}$  from van der Marel (1991), adopting  $F \simeq R$  for bright ellipticals (see Lugger 1989) and computing  $F_\odot$  from the relation V-F=0.40 (B-V) (Kron 1980).

To estimate the virial mass we have evaluated the r.m.s. velocity dispersion  $\sigma_r$  in four concentric rings each containing 1/4 of the galaxies of known redshift of A 2319 A. The four values are  $1148 \text{ km s}^{-1}$ ,  $1415 \text{ km s}^{-1}$ ,  $1327 \text{ km s}^{-1}$ ,  $1193 \text{ km s}^{-1}$  with a r.m.s uncertainty of about  $200 \text{ km s}^{-1}$ . Thus in the following we assume a constant dispersion, derived from the entire A 2319 A sample,  $\sigma_r = 1235 \pm 90 \text{ km s}^{-1}$

The resulting virial mass  $M_V = 3\pi b_G \sigma_r^2 / 2G$  is  $M_V = 2.89 \times 10^{15} h_{50}^{-1} M_\odot$ , namely only 2% less than the value given by OHF, since the decrease of  $\sigma_r^2$  is almost entirely compensated by a

slight increase of the projected virial radius  $b_G = 2\langle 1/b \rangle^{-1}$  (Sarazin 1988), which in our case is  $b_G = 1.736h_{50}^{-1}$  Mpc.

### 3. The gas distribution

From the ROSAT public archive we extracted the available Position Sensitive Proportional Counter (PSPC) images corresponding to two observations of A 2319, on March 1991 and November 1992, which cover a 128x128 arcmin<sup>2</sup> field with pixel size of 15x15 arcsec<sup>2</sup> and an effective resolution of about 25" FWHM, in the energy band 0.5-2.0 keV. The exposure maps (Snowden et al. 1992, Plucinsky et al. 1993), providing the effective exposure time of each pixel, are also available at the ROSAT public archive for each observation. We divided each image for the relevant exposure map and combined the two images with weights proportional to the maxima of the exposure map (1514.6 s and 3200.8 s respectively). The resulting image is shown in Figure 2.

Feretti, Giovannini & Böhringer (1997) (FGB) discuss the radio structure of A2319, which shows a powerful radio halo. They also analyze two substructural features in the X-rays, one corresponds to the E-W elongation in the very center of the A component, detected in the image obtained with the ROSAT High Resolution Imager, and is interpreted by FGB as an evidence of a recent merging process, likely providing the energy for the radio halo. This feature is confined within the inner 5 arcmin and does not affect the analysis of the hydrostatic equilibrium, particularly in the region where the temperature is not constant, i.e. for  $r > 5$  arcmin. In the outer region the cluster structure is rather regular, as for most cD clusters, except for an elongation in the direction of the B component. According to FGB, the B component is in a pre-merger state and has not yet proceed far enough to disturb the bulk of the gas, as can be argued from a comparison with the cluster collision simulation by (Schindler and Müller 1993).

Thus we analyzed A 2319 A as a separate entity, as discussed in section 2. As a first approximation we ignored the presence of the B component, we assumed spherical symmetry and, as in CNT, we derived the volume density  $\rho_{gas}(r)$  of the gas by both numerical inversion of the projection equation, and by fitting the observed surface brightness with a "β-model" (Cavaliere and Fusco-Femiano 1976)  $I(b) = I_0[1 + (b/r_c)^2]^{-3\beta+1/2} + I_b$ , obtaining consistent results. The results are also consistent with FGB and with a more recent analysis of Mohr et al. (1999). Then we applied the same procedure after the exclusion of the northern half ( $\delta > 43^{\circ}56'39''$  (J2000)) of the image, to eliminate the effect of the B component. We have evaluated the constant background value  $I_b = 8.86 \times 10^{-4}$  cts s<sup>-1</sup> arcmin<sup>-2</sup> in the region  $b > 3h_{50}^{-1}$  Mpc. The fitting parameters are reported in Table 2, together with the central proton density  $n_o$ . The one-sigma uncertainties have been evaluated by Monte Carlo simulations, described in section 4. The central proton density is obtained from the relation:

$$I_0[1 + (b/r_c)^2]^{-3\beta+1/2} = EM \cdot \int_{\nu_{min}}^{\nu_{max}} \Lambda(\nu, T) d\nu \quad (3)$$

where  $\Lambda(\nu_{rest}, T)$  is the rest-frame cooling function corrected for the cosmological dimming factor  $(1+z)^4$  and computed with the code of Mewe et al. (1986) with 0.3 solar abundance corresponding to  $\frac{n_e}{n_p} = 1.2$ ,  $\nu_{min}$  and  $\nu_{max}$  define the observing band in the rest-frame and  $EM \equiv \int_0^{\infty} \frac{(n_e)}{n_p} n_o^2 (1 + \frac{r^2}{r_c^2})^{-\frac{3}{2}\beta} dl$  (see Sarazin 1988), and correction for absorption with  $N_H = 8.89 \cdot 10^{-20} \text{ cm}^{-2}$  (Stark et al., 1992) has been applied to  $I_o$ .

Again our results are consistent with the analysis of FGB. In particular we also find a smaller value of the core radius  $r_c$  of the A component when the northern half is excluded to reduce the effect the B component. The observed surface brightness profile and the fitting  $\beta$ -model are shown in Figure 3.

For consistency with the optical analysis, where we eliminated the galaxies assigned to the B component, in the following we adopt the fit obtained after the exclusion of the northern half of the cluster image. The corresponding gas density profile  $\rho_{gas}(r) = \rho_{gas}^0 [1 + (b/r_c)^2]^{-3\beta/2}$  is obtained assuming a constant temperature equal to the emission-weighted temperature  $T_X = 10.0 \pm 0.7 \text{ keV}$  (Markevitch 1996). The non-isothermality does not significantly affect the results (Markevitch et al. 1996), due to the weak dependence of the emissivity on temperature, in the adopted band (see next section). The gas density profile has been computed also by a non parametric numerical deprojection as in CNT, obtaining consistent results.

#### 4. Hydrostatic model, mass distributions and baryon fraction

As pointed out in CNT, it is possible to check the hydrostatic equilibrium condition in a non-parametric way, by a direct comparison of the density profiles of gas and galaxies. Assuming spherical symmetry, the equilibrium condition implies (Bahcall and Lubin 1994):

$$\frac{\mu m_p \sigma_r^2}{kT} = \frac{d \ln \rho_{gas}(r) / d \ln r + d \ln T / d \ln r}{d \ln \rho_{gal}(r) / d \ln r + d \ln \sigma_r^2 / d \ln r + 2A} \quad (4)$$

where  $\sigma_r$  is the radial galaxy velocity dispersion,  $A = 1 - \left(\frac{\sigma_t}{\sigma_r}\right)^2$  measures the anisotropy of the velocity distribution and  $\mu$  is the average molecular weight which we assume equal to 0.58 (Edge and Stuart 1991). For constant  $\sigma_r$  and  $T$ , and  $A = 0$ , this implies  $\rho_{gas} \propto \rho_{gal}^\beta$  where  $\beta_{spec} = \frac{\mu m_p \sigma_r^2}{kT}$  is a constant representing the ratio between the energy per unit mass in the galaxies and the gas respectively (Cavaliere and Fusco-Femiano 1976). In this case it is possible to define the morphological parameter  $\beta_{XO} \equiv d \ln \rho_{gas}(r) / d \ln \rho_{gal}$  to be compared with  $\beta_{spec}$  which is obtained from the spectroscopic observation of galaxies and the gas temperature derived from X-ray spectra. As already discussed in CNT, the very existence of a wide range of densities where  $\beta_{XO}$  is constant supports, in many cases, the validity of the isothermal model. However in the presence of a temperature gradient, as in the case of A 2319 A, both  $\beta_{spec}$  and  $\beta_{XO}$  depend on radius and the equilibrium equation reads:

$$\beta_{spec} = \beta_{XO} + \beta_{TO}, \quad (5)$$

where  $\beta_{TO} \equiv d \ln T / d \ln \rho_{gal}$  and we still assume that the galaxy velocity distribution is isotropic and  $\sigma_r$  is constant. To check the validity of equation 5 we used the temperatures obtained by Markevitch 1996. We computed  $\beta_{spec}$ ,  $\beta_{XO}$  and  $\beta_{TO}$  at three projected radii of 4, 10 and 20 arcmin, corresponding to the boundaries of the four rings whose temperatures are given by Markevitch 1996. With the constant velocity dispersion  $\sigma_r = 1235 \pm 90 \text{ km s}^{-1}$  derived in section 2,  $\beta_{spec}$  ranges from  $0.86 \pm 0.15$  in the first point, to  $1.52 \pm 0.47$  in the outermost point, i.e. the ratio between the energy per unit mass in gas and galaxies is close to unity within a central isothermal region of about  $0.5 \text{ h}_{50}^{-1} \text{ Mpc}$ , while it decreases in the outer regions.

Figure 4 shows  $\ln \rho_{gas}$ , obtained by numerical deprojection, versus  $\ln \rho_{gal}$ . From the slope of the curve is possible to derive a value of  $\beta_{XO}(r)$  at each radius.

The values of  $\beta_{XO}(r)$  range from  $0.59 \pm 0.06$  in the first ring, to  $0.64 \pm 0.06$  in the outermost ring. The one-sigma uncertainties are evaluated from Monte Carlo simulations described below. We also computed  $\beta_{TO}(r)$ , which is close to zero in the cluster center and increases up to  $0.58 \pm 0.44$  at  $r \approx 1 \text{ h}_{50}^{-1} \text{ Mpc}$ . The one-sigma uncertainties are derived from errors on the temperature values reported in Figure 2 of Markevitch 1996. Figure 5 shows  $\beta_{spec}(r)$  as a function of the RHS of equation 5,  $(\beta_{XO} + \beta_{TO})$ .

We stress that the relation between the two quantities on the x and y axes is not automatically implied by their definition, since the galaxy density  $\rho_{gal}(r)$  only appears in the RHS and is observationally independent of the quantities in the LHS.

The value of  $\beta_{spec}(r)$  is slightly larger than  $\beta_{XO} + \beta_{TO}$ . This could indicate that  $\sigma$  is still slightly overestimated due to the presence of the background component A 2319 B. However the intrinsic statistical uncertainty does not allow this level of accuracy. Furthermore, even small deviation from the spherical symmetry, or from isotropy of the velocity distribution, could have comparable effects.

All we can safely say is that there is an increase of  $\beta_{spec}$  versus  $(\beta_{XO} + \beta_{TO})$ , which is consistent with a straight line of unit slope. Thus, within the present uncertainties the data are consistent with equation 5, namely with validity of the hydrostatic equilibrium, also in the outer region of the cluster where the temperature declines.

The accuracy of this type of check, as applied to a single cluster, is limited by various factors. Although future X-ray data will provide much higher signal-to-noise, the uncertainty on galaxy density profile is intrinsically limited by Poisson noise on galaxy counts. Moreover subclustering and unknowable deviations from spherical symmetry will always produce an uncertainty on the galaxy density deprojection.

Nevertheless, the systematic application of the method described, to all the cluster with measured temperature distribution (Markevitch et al. 1998) will likely provide statistical indication on the validity of, or the deviation from, the equilibrium conditions in the outer parts of galaxy clusters.

Assuming that our results indicate the validity of hydrostatic equilibrium, we can derive the distribution of the total binding mass  $M_T(r)$  of A2319A:

$$M_{tot}(r) = -\frac{kT}{\mu m_p G} \left( \frac{d \ln \rho_{gas}(r)}{d \ln r} + \frac{d \ln T}{d \ln r} \right) r \quad (6)$$

The slopes of the temperature profiles are crucial in establishing whether the non-isothermality causes an increase or decrease of the mass estimate, with respect to the isothermal  $\beta$ -model.

In fact, from equation 6, indicating with  $M_{tot}^{isot}(r)$  the mass derived by an isothermal  $\beta$ -model with temperature  $T_{isot}$  the fractional change in the mass estimate is:

$$\Delta(r) \equiv \frac{M_{tot}(r) - M_{tot}^{isot}(r)}{M_{tot}^{isot}(r)} = \frac{T(r) - T_{isot}}{T_{isot}} + \frac{T(r)}{T_{isot}} \frac{d \ln T}{d \ln \rho_{gas}} \quad (7)$$

where the two terms on the r.h.s. of the equation can be of the same order.

It is customary to adopt a polytropic gas distributions as the simplest analytic representation of a non-isothermal gas in hydrostatic equilibrium. In this case  $T \propto \rho_{gas}^{\gamma-1}$ , with the polytropic index  $\gamma$  ranging from unity to 5/3 for an isothermal or adiabatic equilibrium respectively. The polytropic model implies (Cowie, Henriksen and Mushotzky 1987):

$$\begin{aligned} \rho_{gas}(r) &= \rho_{gas}^o [1 + (r/r_c)^2]^{-\delta}, & T(r) &= T_o [1 + (r/r_c)^2]^{-\alpha}, \\ \delta &= \frac{3\beta/2}{1 + \eta(\gamma-1)/2}, & \alpha &= \delta(\gamma-1) \end{aligned} \quad (8)$$

where  $\eta \equiv d \ln \epsilon / d \ln T$  and  $\epsilon$  is the emissivity of the gas, integrated in the adopted band. We can fit the temperature profile of A 2319 provided by Markevitch 1996, neglecting the effect of projection and adopting  $\eta \simeq -0.2$ , to determine the polytropic index  $\gamma$ . Notice that, due to small value of  $\eta$ , the result is not significantly different if we simply assume  $\delta = 3\beta/2$  and  $\eta = 0$  in the above expressions. The slope  $|dT/dr|$  of the temperature profile reaches a maximum at  $r/r_c = -\alpha + \sqrt{\alpha^2 + 1}$  and progressively decreases in the outer regions.

As a result, for  $T_{isot} = T_o$ , the quantity  $\Delta(r)$  is positive only for  $r/r_c < x_\gamma \equiv \sqrt{\gamma^{1/\alpha} - 1}$ . This limit decreases for increasing  $\beta$  and  $\gamma$ , e.g.  $x_\gamma \simeq 0.78$  for  $\beta = 1$ ,  $\gamma = 5/3$  and  $\eta = -0.2$ , while  $x_\gamma = \sqrt{e^2 - 1} \simeq 2.53$  for  $\beta = 1/3$  and  $\gamma = 1$ . We stress that  $\Delta(r)$  is always negative at large radii, and this implies an enhancement of the “baryon catastrophe”. The best fit value is  $\gamma = 1.091$  and the resulting temperature profile is shown in Figure 6.

The quality of the fit is quite poor, and there is a probability of 91% that the deviations are non random. The increment of the mass in the central region, with respect to isothermal model, and the enhancement of the baryonic catastrophe obtained with a polytropic model are a mere artifact of the particular shape of the polytropic temperature profile, which is not a good representation of the data, at least in the case of A 2319 A.

More specifically, the data seem to indicate an almost isothermal central region and an increasing slope of the temperature profile for increasing radius.

This behavior is consistent with a change of the polytropic index with radius from an isothermal ( $\gamma = 1$ ) towards an adiabatic ( $\gamma = 5/3$ ) hydrostatic equilibrium (see Sarazin 1988). A fit with the law  $T(r) = T_o - ar^2$  is shown in Figure 6. In this case the probability is  $P(> \chi^2) = 0.99$ .

Figure 7 shows  $M_{tot}^{isot}(r)$ , corresponding to the isothermal model, and  $M_{tot}(r)$  as obtained with both the polytropic model and the quadratic interpolation of the temperature profile. On the basis of the above discussion we assume the latter as the best representation of the mass distribution.

In the same figure, galaxy and gas masses,  $M_{gal}(r)$  and  $M_{gas}(r)$  are also shown. The latter is computed both in the isothermal approximation and using the temperature profile: the result is only weakly dependent on the temperature changes.

$M_{gas}(r)$  is steeper than  $M_{gal}(r)$  and  $M_{tot}(r)$ , which have more similar slopes. As a consequence the gas mass dominates over the galaxy mass at large radii. These results are consistent with previous findings of CNT.

The statistical uncertainties have been evaluated by Monte Carlo simulations of the entire reduction process. For the X-ray data, starting from a "β-model" corresponding to the fitting parameters, we generated 500 random sets representing the photon counts in each radial ring with Poisson noise, and we extracted 500 random background values, with a standard deviation estimated from intensity fluctuation of the surface brightness outside  $3h_{50}^{-1}$  Mpc where the background value has been measured. Then we fitted with a "β-model" each intensity profile, obtaining the statistical distribution of the fitting parameters. Finally we extracted 500 values of the temperature in each of the four rings corresponding to the data of Markevitch 1996, with the relevant standard deviations, and we fitted the temperature profile with a parabolic law. Then we applied to the simulated data the same algorithms applied to real data for the evaluation of the mass profiles. This procedure allows to define a one-sigma confidence interval for the gas mass  $M_{gas}$  and for the total mass  $M_{tot}$  as a function of radius. A similar procedure was adopted for the galaxy distribution. Then we extracted, for each cluster simulation, a random value of  $M/L_{F_\odot}$  from a gaussian distribution with a mean value and a standard deviation corresponding obtained from van der Marel (1991). The one-sigma confidence intervals are reported as shaded areas in Figure 7.

We define the luminous mass as the sum of the gas mass and the galaxy mass as deduced using an average stellar mass-to-light ratio (see section 2):  $M_{lum} = M_{gas} + M_{gal}$ . The above results imply that the dark matter  $M_{dark} = M_{tot} - M_{lum}$  has a distribution similar to  $M_{gal}(r)$ . This provides a constraint on the mechanism of galaxy and cluster formation.

Since an unknown fraction of the dark matter is baryonic,  $M_{lum}/M_{tot}$  represents a lower limit on the baryon fraction  $f_b$ . Figure 8 shows this lower limit as a function of radius, as computed in the isothermal approximation and taking into account the temperature gradient by the polytropic

model and by the quadratic interpolation. We can compare our estimate of  $f_b$  with the results of Mohr et al. (1999) who gives the  $f_b$  values  $f_b = 0.213 \pm 0.004$  and  $f_b = 0.297 \pm 0.027$ , at  $1h_{50}^{-1}$  Mpc and at  $1.91h_{50}^{-1}$  Mpc respectively, the latter distance representing  $r_{500}$ , namely the radius within which the mean density is 500 times the critical density  $\rho_{crit} = 3H_o^2/8\pi G$ . Our isothermal values  $f_b = 0.180 \pm 0.017$  and  $f_b = 0.252 \pm 0.045$  are slightly lower, because were derived by a fit of the southern part of the X-ray image, to exclude the effect of the B component.

At  $2 h_{50}^{-1}$  Mpc  $f_b$ , as computed with the quadratic interpolation, becomes respectively 66 % and 56 % of the isothermal and polytropic values, thus mitigating the "baryon catastrophe".

Assuming  $f_b \simeq 0.2$  as typical of galaxy clusters, the residual discrepancy between  $\Omega_b = f_b\Omega_o$  and the corresponding value derived from nucleosynthesis calculations  $\Omega_b^{nucl} \simeq 0.076 \pm 0.004h_{50}^{-2}$  (Burles and Tytler 1998), can be reconciled assuming  $\Omega_o < \Omega_b^{nucl}/f_b \lesssim 0.4$ .

## 5. Summary and Conclusions

We have performed a new analysis of the Abell cluster A 2319, and assigned the individual galaxies to the A 2319 A and A 2319 B components by an objective criterion taking into account both position and redshift. The resulting velocity dispersion of the A component is slightly smaller, but consistent with the previous determination of OHF.

We have obtained photographic F band photometry of the cluster galaxies, which allows us to construct the cluster luminosity function and galaxy density profile.

We have analyzed archival ROSAT PSPC images separating the A component on the basis of the optical information, and we have obtained a gas density profile of the A component. The result is consistent with recent studies of Feretti, Giovannini and Böhringer (1997), Mohr et al. (1999).

Since, according to Markevitch 1996, A 2319 A shows a radial gas temperature decrease, we have generalized the method introduced by Cirimele, Nesci & Trèvese (1997) CNT, in order to check the validity of the hydrostatic equilibrium in the case of a non isothermal gas.

We have derived the total mass profile  $M_{tot}(r)$  through the non isothermal hydrostatic equation adding new evidence in favor of the results of CNT that the total mass and the galaxy mass have similar radial distributions, more concentrated with respect to the gas component.

Polytropic models imply smaller masses at large radii, respect to the isothermal model, i.e. a higher value of the baryon fraction. Thus, the use of a polytropic model would enhance the baryon catastrophe.

However we have shown that the polytropic model is inconsistent with the observed temperature profile, at least in the specific case of A 2319 A. A parabolic representation of the temperature profile gives, instead, a total mass larger than computed in the isothermal

approximation, mitigating the baryon catastrophe.

In any case,  $f_b$  is larger than  $\Omega_b^{nucl} \simeq 0.076 \pm 0.004 h_{50}^{-2}$ , resulting from nucleosynthesis calculations and recent measures of the deuterium to hydrogen ratio (D/H), in high resolution studies of the  $Ly\alpha$  forest (Burles and Tytler 1998). Under the assumption that the value of  $f_b \approx 0.2$ , found for A 2319 A, which is consistent with other estimates (Evrard 1997, CNT, Ettori & Fabian 1999, Mohr et al., 1999) is typical of galaxy clusters, it is possible to derive the following conclusions. If the  $\Omega_o = 1$  assumption is kept, then the baryonic fraction within galaxy clusters is not representative of the cosmic value and clusters must be surrounded by dark matter halos (White and Fabian 1995). If, on the other hand, beyond  $r \approx 2h_{50}^{-1}$  Mpc the material has not yet fallen into the cluster, as infall models indicate, then  $f_b$  is representative of the cosmic value and the cosmological parameter must be  $\Omega_o = \Omega_b^{nucl}/f_b$  (White et al. 1993 and refs. therein), i.e. in our case  $\Omega_o \lesssim 0.4$ , where the uncertainty on the latter value depends on the intrinsic spread of the baryon fraction, in the presently observable volumes around galaxy clusters.

Recently Markevitch et al. (1998) have collected temperature profiles for 30 galaxy clusters based on ASCA observations. However, only a minority of clusters is regular enough, specially in the outer regions, to allow an X-ray and optical check of the equilibrium conditions as suggested in the present paper. This limits the accuracy and the reliability of a “measure” of the cosmological parameter  $\Omega_o$ , based on a comparison between the baryon fraction  $f_b$  and  $\Omega_b^{nucl}$ . Moreover future cosmic microwave background experiments are expected to provide tighter constraints on  $\Omega_o$  (Mandolesi et al. 1995) as compared with the results derived from the analysis of the matter distribution in galaxy clusters.

On the basis of this new estimate of  $\Omega_o$ , once the equilibrium conditions of the non-isothermal regions are verified by the systematic application of the analysis outlined in the present paper, it will be possible to extend the (otherwise questionable) estimates of the general distribution of luminous and dark matter based on the hydrostatic model, to the outer regions of galaxy clusters of a statistical sample, thus providing new constraints for the models of cluster formation and the physics of large scale baryon segregation.

We are grateful to the anonymous referee and to the editor for comments and suggestions. This work has been partly supported by Ministero dell’Università e della Ricerca Scientifica e Tecnologica (MURST).

Table 1. Galaxy density fits.

de Vaucouleurs profile				
$\sigma_0$ (kpc $^{-2}$ )	$r_v$ (kpc)	$\gamma_g$	$\sigma_b$ (deg $^{-2}$ )	$P_{KS}(> D)$
$(0.67 \pm 0.3) \cdot 10^{-1}$	$259 \pm 104$	$0.16 \pm 0.03$	$17 \pm 10$	0.70

King profile				
$\sigma_0$ (kpc $^{-2}$ )	$r_c$ (kpc)	$\kappa$	$\sigma_b$ (deg $^{-2}$ )	$P_{KS}(> D)$
$(0.43 \pm 0.19) \cdot 10^{-3}$	$39 \pm 15$	$0.690 \pm 0.14$	$19 \pm 11$	0.79

Table 2. X-ray brightness fits.

<i>Image</i>	$I_o \times 10^4$ $cts s^{-1} arcmin^{-2}$	$n_o \times 10^3$ $cm^{-3}$	$r_c$ $Mpc$	$\beta$	$\chi^2/\nu$
Overall <sup>a</sup>	801±144	5.28±0.70	0.213±0.090	0.518±0.070	174/62
Southern <sup>a</sup>	950±171	6.62±0.84	0.159±0.071	0.511±0.069	82/62

<sup>a</sup>For both images exposure time is 4715.4 s and the background is  $I_b = 8.86 \cdot 10^{-4} cts s^{-1} arcmin^{-2}$

## REFERENCES

Abell, G.O., Corwin, R.P., Olowin, R. P. 1989, *ApJS*, 70, 1

Arnaud, C. W. 1994, *ApJ*, 436, L67

Bahcall N. A., & Lubin L. M. 1994, *ApJ*, 426, 513

Briel, U. G., Henry, J. P., & Böhringer, H. 1992, *A&A*, 259, L31

Burles, S. & Tytler, D., 1998, *ApJ*, 507, 732

Cavaliere A., & Fusco-Femiano R. 1976, *A&A*, 49, 137

Cirimele, G., Nesci, R., & Trèvese, D. 1977, *ApJ*, 475, 11 (CNT)

Cowie, I. L., Henriksen, M., & Mushotzky, R. 1987, *ApJ*, 317, 593

David L. P., Arnaud K. A., Forman W., Jones C. 1990, *ApJ*, 356, 32

David L. P., Jones C., Forman W. 1995, *ApJ*, 445, 578

Dressler, A., & Shectman, S. A. 1988, *AJ*, 95, 985

Durret, F., Gerbal, D., Lachièze-Rey, M., Lima-Neto, G., & Sadat , R. 1994, *A&A*, 287, 733

Edge, A. C., and Stuart, G. C. 1991, *MNRAS*, 252, 428

Ettori, S., & Fabian, A. C. 1998, *MNRAS*, 293, L33

Ettori, S., & Fabian, A. C. 1999, *MNRAS*, 305, 834

Evrard,A. E. 1997, *MNRAS*, 292, 289

Evrard,A. E. 1990, in STScI Symp. 4, Clusters of Galaxies, ed. Oegerle et al., (Cambridge: Cambridge Univ. Press), 287

Faber, S. M., & Dressler, A. 1977, *AJ*, 82, 187

Fabian, A.C., Nulsen, P.E., & Canizares, C.R. 1984, *Nature*, 310, 733

Feretti, L., Giovannini, G., & Böringer, H. 1997 *New Astronomy*, 2, 501 (FGB)

Flin,P., Trévese, D., Cirimele, Hickson, P. 1995, *A&AS*, 110, 313

Gerbal, D., Durret, F., Lima-Neto, G., & Lachièze-Rey, M. 1992 *A&A*, 253, 77

Hughes, J. P., Gorenstein, P., & Fabricant, D. 1988, *ApJ*, 329, 82

Hughes, J. P. 1989, *ApJ*, 337, 21

Ikebe, Y et al. 1996, *Nature*, 379, 427

Jones C., & Forman W. 1984, *ApJ*, 276, 38

Mandolesi, N. et al. 1995, *Planetary and Space Science*, 43, 1459

Kron, R. G., 1980, *ApJS*, 43, 305

Lugger, P.M., 1989, *ApJ*, 343, 572

Markevitch, M. 1996, *ApJ*, 465, L1

Markevitch, M., Forman W. F., Sarazin C. L., & Vikhlinin A. 1998, *ApJ*, 503, 77

Markevitch, M., Mushotzky, R., Inoue, H., Yamashita, K., Furuzawa, A., and Tawara, Y. 1996, *ApJ*, 456, 437

Markevitch, M., Yamashita, K., Furuzawa, A., & Tawara, Y. 1994, *ApJ*, 436, L71

Mewe, R., Lemen, J. R., & van den Oord, G. H. J., 1986, *A&AS*, 65, 511

Molendi, S. 1998, in *Dark Matter*, ed Salucci P. (Firenze: Studio Editoriale Fiorentino)

Molendi, S. et al., *astro-ph/9909228*

Mohr, J.J., Mathissen, B., & Evrard, A.E., 1999, *ApJ*, 517, 627

Oegerle W.R., Hill J.M., & Fitchett M.J. 1995, *AJ*, 110, 32 (OHF)

Olive K.A., Steigman G. 1995, *ApJS*, 97, 49O

Plucinsky, et al. 1993, *ApJ*, 418, 519

Sarazin, C. 1986, *Rev. Mod. Phys.* 58, 1

Sarazin, C. L. 1988, "X-ray emissions from clusters of galaxies", Cambridge Univ. Press

Schechter, P. 1976, *ApJ*, 203, 297

Schindler, S., & Müller, E. 1993, *A&A*, 272, 137

Snowden, et al. 1992, *ApJ*, 393, 819

Stark, A.A., Gammie, C. F., Wilson, R. W., Bally, J., Linke, R. A., Heiles, C., & Hurwitz, M., 1992, *ApJS*, 79, 77

Trèvese, D., Flin, P., Migliori, L., Hickson, P., & Pittella G. 1992, *A&AS*, 94, 327

Trèvese, D., Cirimele, & Appodia, B. 1996, *A&A*, 315, 365

Trèvese, D., Cirimele, G., & Flin, P. 1992, AJ, 104, 3

Trèvese, D., Cirimele, G., Cenci, A., Appodia, B., Flin, P., & Hickson, P. 1997, A&AS, 125, 459

van der Marel, R. P., 1991, MNRAS, 253, 710

Walker, T. P., Steigman, G., Schramm, D. N., Olive, K. A., & Kang, H. 1991, ApJ, 376, 51

White S. D. M., and Fabian A. C. 1995, MNRAS, 273, 72

White, D. A., Jones, C., & Forman, W. 1997, MNRAS, 292, 419

White, S. D. M., Navarro, J. F., Evrard, A. E., & Frenk, C. S. 1993, Nature, 366, 429

Fig. 1.— Radial profile of the surface density of galaxies. Vertical bars represent the standard deviation of the number counts in the relevant annulus. The curves represent the fits of unbinned data. *Solid line*: King profile; *dotted line*: de Vaucouleurs profile.

Fig. 2.— ROSAT/PSPC image of A 2319. The image is filtered with a gaussian of 100 arcsec (FWHM). The contour levels, starting from  $0.40 \text{ counts pixel}^{-1}$  ( $1\text{pixel} = 15'' \times 15''$ ) increase by a factor  $2^{1/2}$ . Notice the asymmetry in the N-NW direction, due to the B component.

Fig. 3.— X-ray surface brightness profile of A 2319 A, after the exclusion of the northern half of the image. Errors represent the standard deviation of photon counts. The solid line is the fit with the  $\beta$ -model.

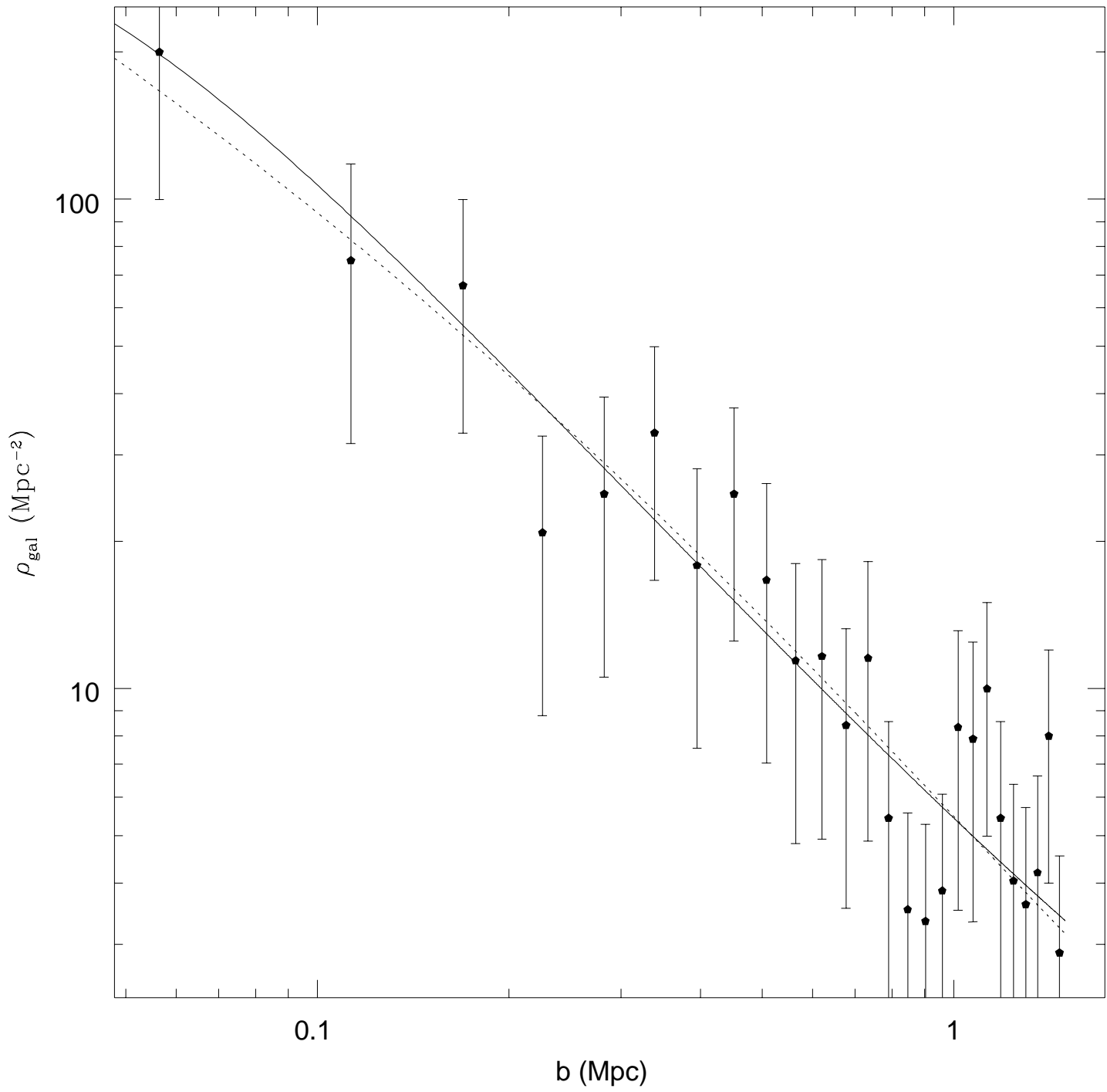
Fig. 4.— The gas density  $\rho_{\text{gas}}(r)$ , derived from numerical inversion of the projection equation (see CNT), versus the fitted galaxy density  $\rho_{\text{gal}}(r)$ . Vertical lines show the relevant radii, indicated in Mpc ( $h_{50} = 1$ ). The local slope of the curve defines the function  $\beta_{XO}(r)$ .

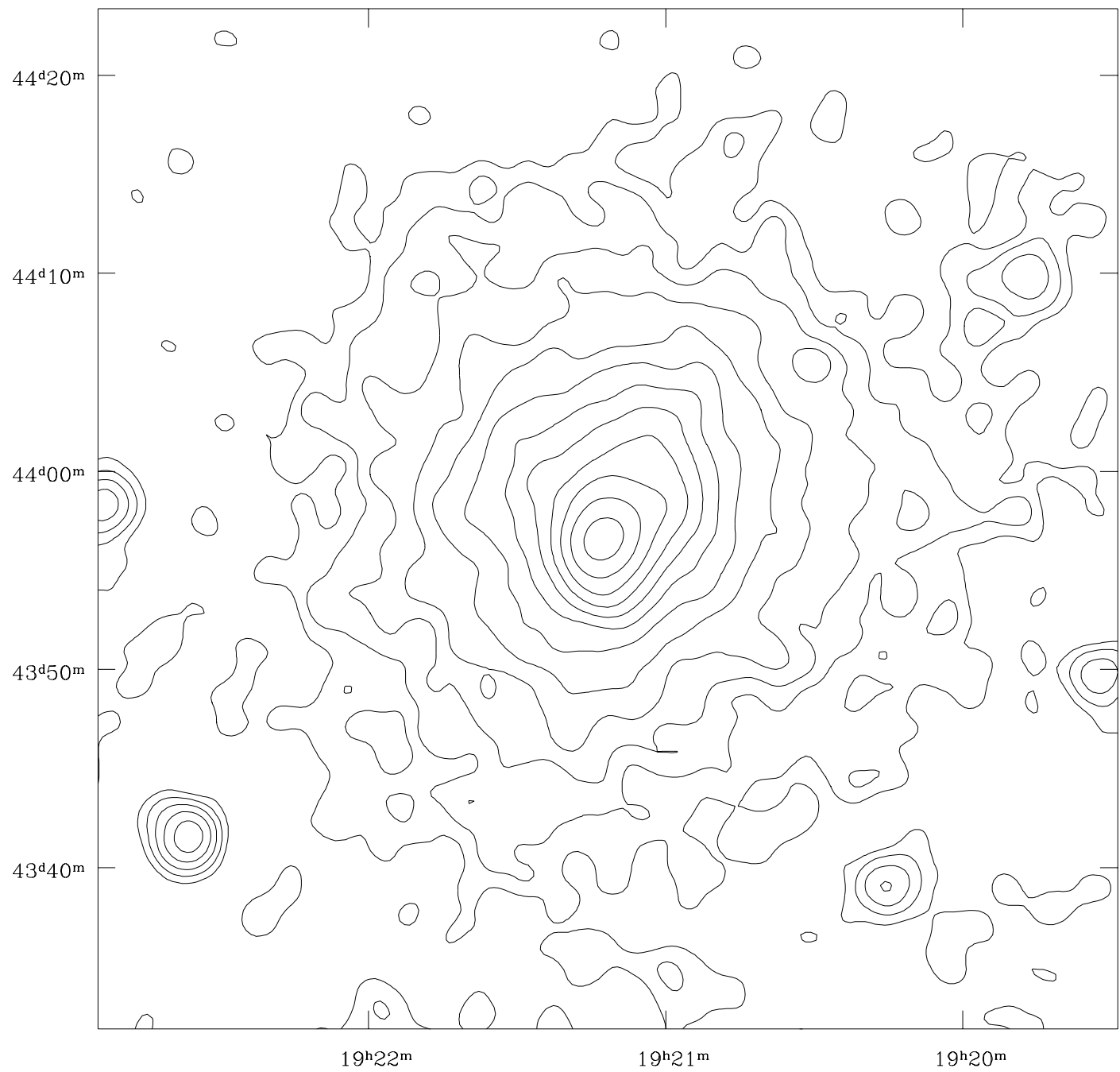
Fig. 5.—  $\beta_{\text{spec}}$  versus  $(\beta_{XO} + \beta_{TO})$  computed at the radii of 4, 10, 20 arcmin, corresponding to the boundaries of the four rings whose temperatures are given by Markevitch (1996).

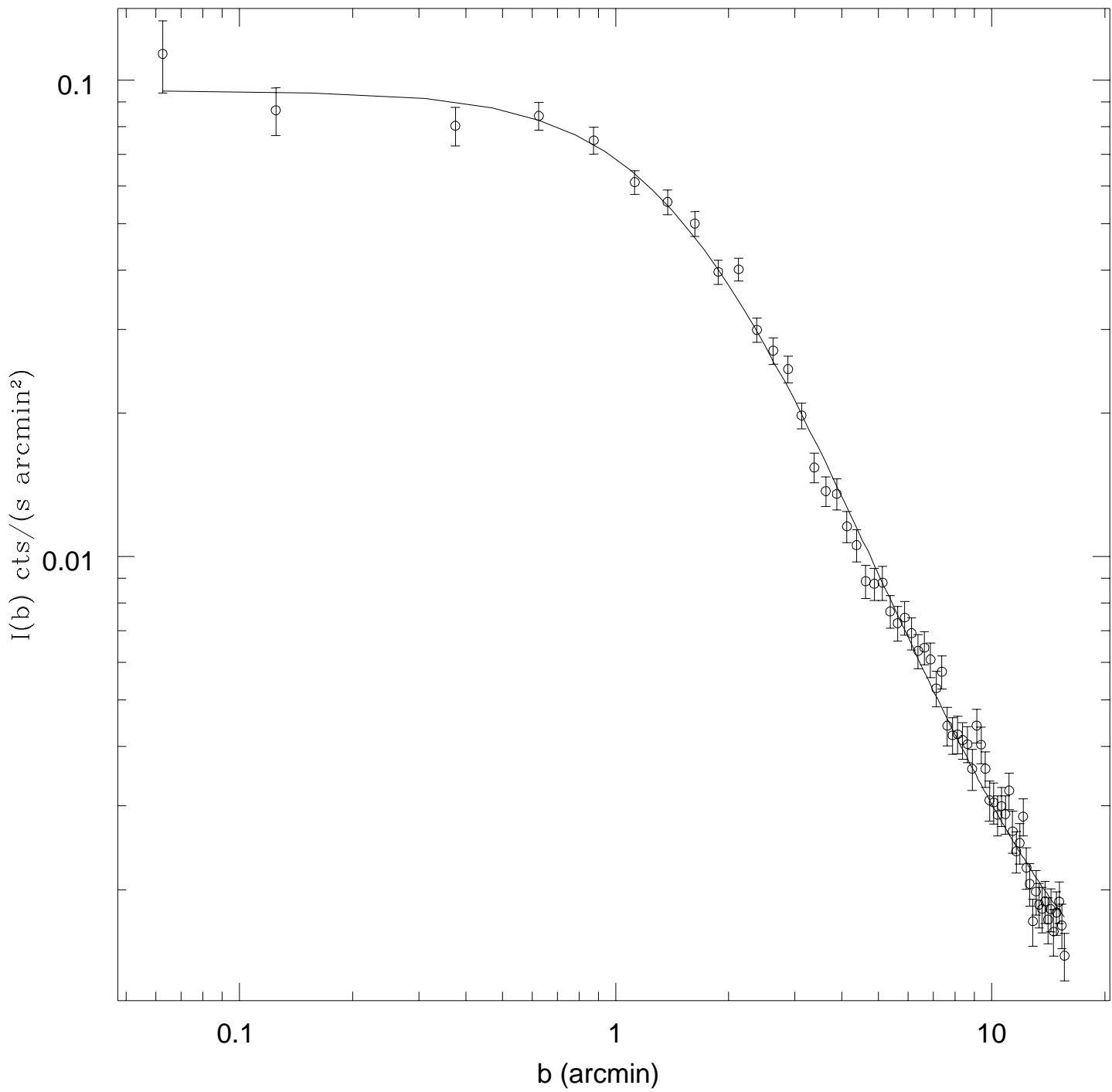
Fig. 6.— Temperature versus radius of A 2319 A, as deduced from Markevitch (1996). *dotted*: best fit polytropic model; *short dash*: quadratic interpolation  $T(r) = T_o + ar^2$ .

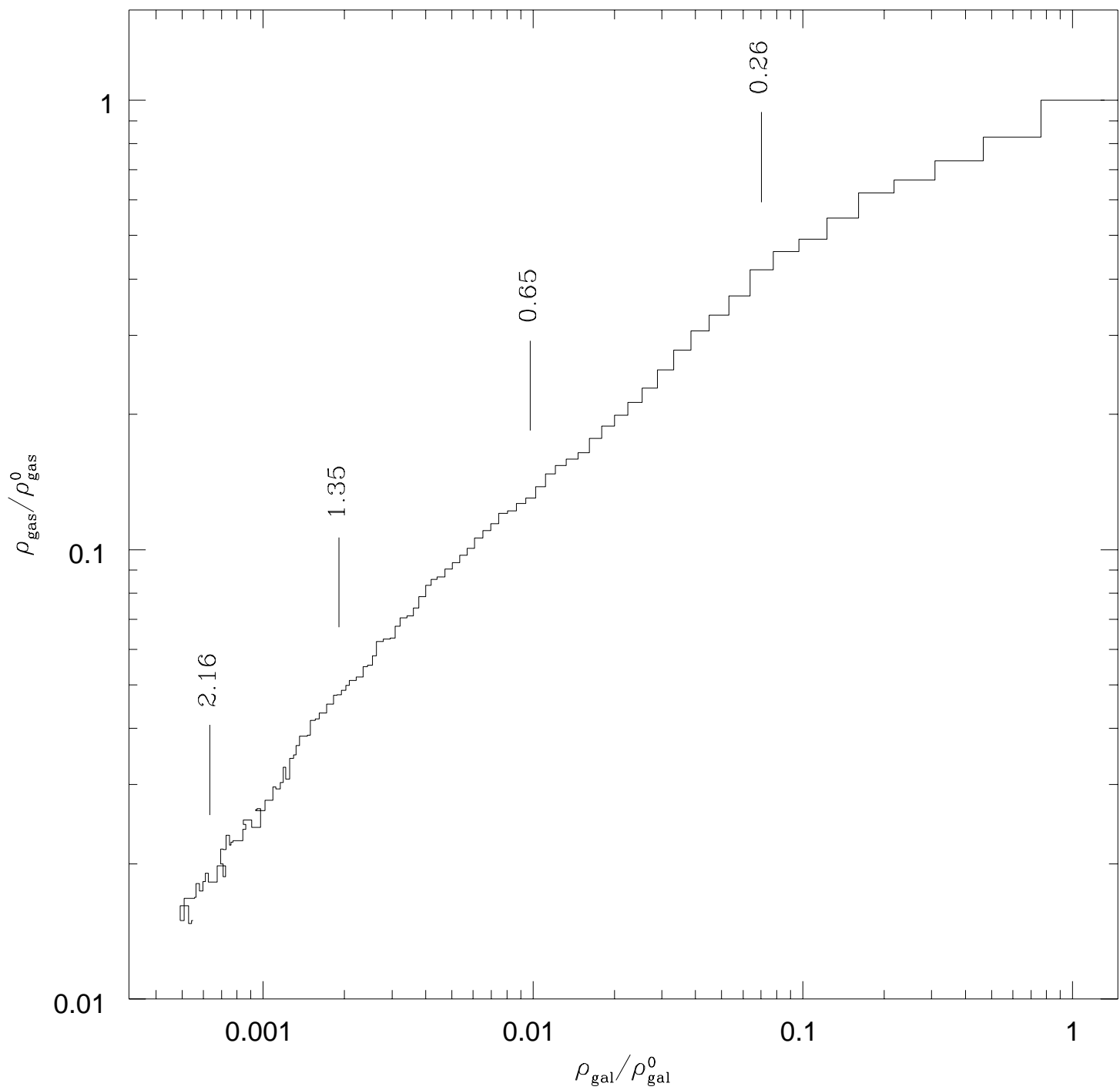
Fig. 7.— The mass as a function of radius for A 2319 A. *Solid*: total binding mass  $M_{\text{tot}}^{\text{isot}}(r)$ , for the isothermal “ $\beta$ ”-model with  $T_{\text{isot}} = 10 \pm 0.7 \text{ keV}$ ; *dotted line*:  $M_{\text{tot}}(r)$  for the polytropic model; *shaded area*:  $M_{\text{tot}}(r)$  for  $T(r) = T_o - ar^2$ ; *long dash*: galaxy mass  $M_{\text{gal}}(r)$ ; *dot dash*: gas mass  $M_{\text{gas}}(r)$ . Shaded areas represent the  $1\sigma$  uncertainty as deduced by Monte Carlo simulations.

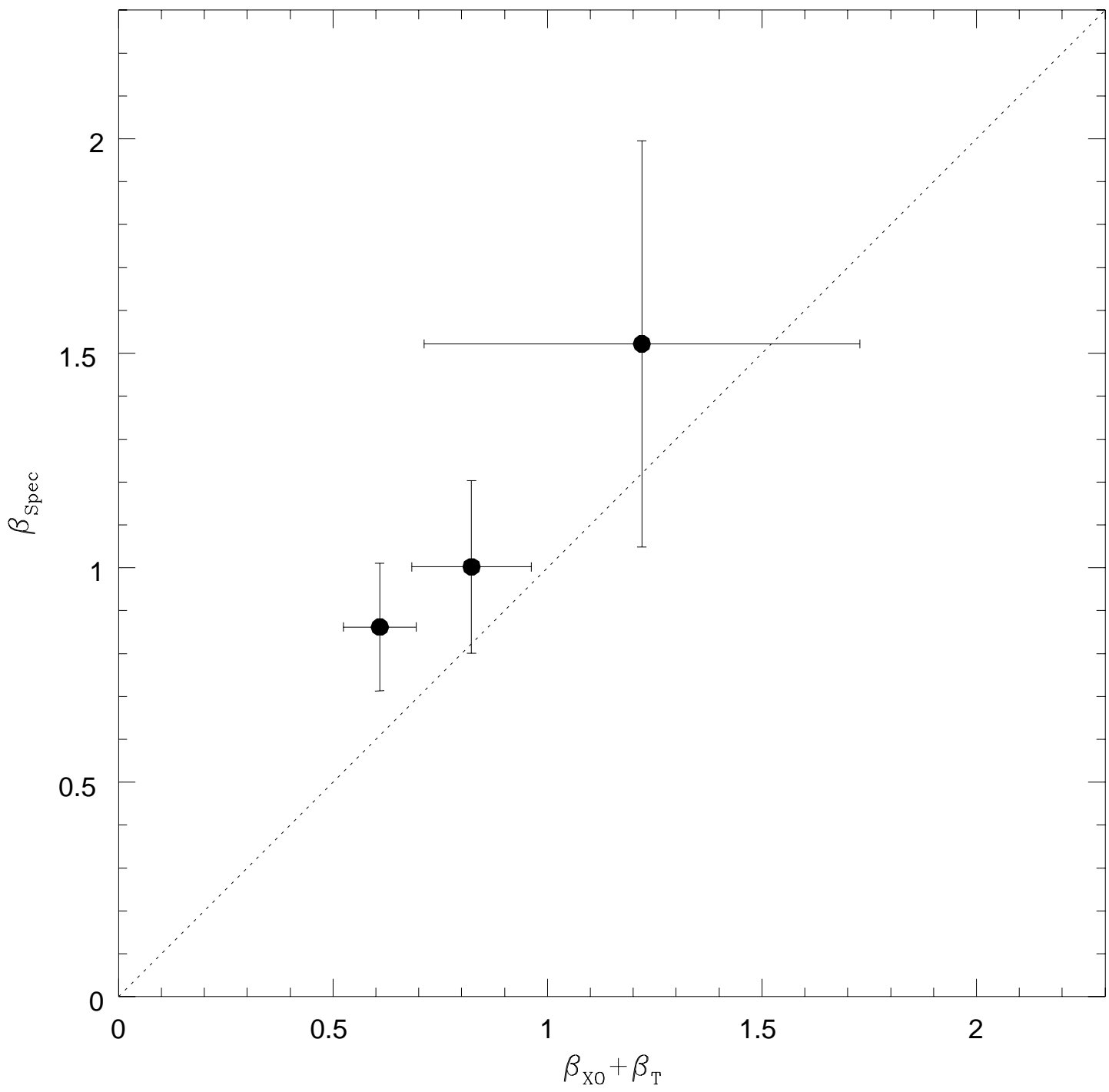
Fig. 8.— Baryon fraction  $f_b(r)$  as a function of radius. *Solid*: isothermal “ $\beta$ -model”; *dotted*: polytropic model; *shaded area*: model with  $T(r) = T_o - ar^2$  with the  $1\sigma$  uncertainty as deduced by Monte Carlo simulations.

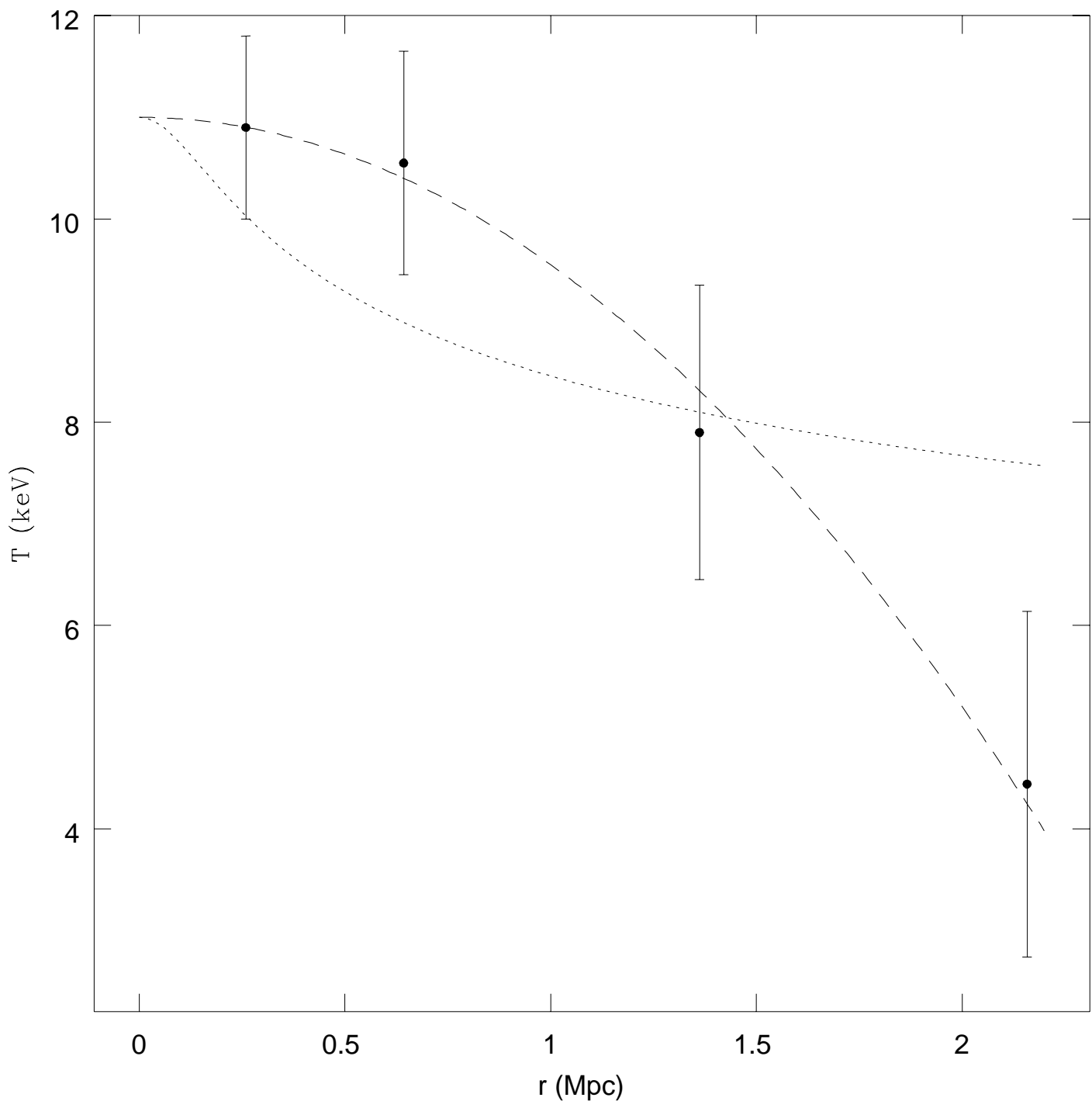












A2319A

